北京正负电子对撞机国家实验室

2001

北京同步辐射装置用户科技论文集

（上册）

北京正负电子对撞机国家实验室办公室编印

北京正负电子对撞机国家实验室

北京同步辐射装置用户科技论文集

上 册

北京正负电子对撞机国家实验室办公室编印

2001年4月

序

2000-2001 运行年度，BSRF 的工作一直得到广大用户的极大支持和关爱，使我们的工作又有长足的进展。同步辐射专用运行机时增加，光源质量进一步改善，课题管理更加完善，研究领域有所扩展，研究水平不断提高。经过多年的积累，许多研究课题取得了丰硕的成果，有的课题取得了重大突破，一些具有创新性、高难度的课题也取得了不同程度的进展。

为了促进 BSRF 与国内、外科学家的交流合作，也作为 BSRF 工作的鞭策。我们从 1997 年起收集用户和 BSRF 工作人员在 BSRF 上全部或部分实验发表的论文。每年编辑一册 "北京同步辐射装置上的科学研究论文集"。 2001 年在国内外学术杂志上发表论文 131 篇(不完全统计)，本论文集共收集用户论文 102 篇，其中 SCI 收录 110 余 篇，影响因子 1—1.5 的 19 篇，1.5—2.0 的 10 篇，大于 2 的 8 篇。本论文集是 2000-2001 运行年度 BSRF 科研工作的缩影，是广大用户和 BSRF 工作人员辛勤劳动和聪明才智的结晶。在此，我们感谢为 BSRF 发展做出贡献的广大用户和 BSRF 工作人员。由于各种原因，可能还有一些高水平的论文没有收集到 "论文集" 中，我们谨向这些论文的作者表示深深的歉意。

另有部分文章已在“高能物理与核物理” 2001 年增刊刊载，为了避免重复，本文集只登录文章目录，原文请见高能物理与核物理(GAONENG WULI YU HEWULI) 第 25 卷 增刊。

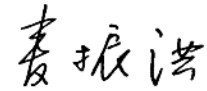

2001 年 4 月

北京同步辐射装置用户 2001 年科技论文目录

(上　册)

【EXAFS 实验站】

【真空紫外光谱实验站】

【光电子谱学实验站】

【荧光分析实验站】

Local structure of NiTi nanocrystals studied by EXAFS and XRD

Xin JU, Yixi SU

Institute of High Energy Physics, Chinese Academy of Sciences, Beijing 100039, P. R. China, Email: jux@alpha02.ihep.ac.cn

A series of NiTi nanocrystals with different annealing temperatures, prepared by sputtering method, were investigated by extended x-ray absorption fine structure (EXAFS) and x-ray diffraction. It was found that the structure of nano-phase powder is different from bulk NiTi alloy with bcc structure as target materials. When increasing the annealing temperature, a small fraction of the (Ni,Ti) type nanocrystal with the hexagonal structure was presented except target materials and Ni, and it is atomic occupation in random. Finally there were four Ti and two Ni atoms around central Ni atoms, and the bond length of Ni-Ti and Ni-Ni were 0.2462nm and 0.2585nm at 800°C annealed.

Keywords: NiTi nanocrystals, Phase transition

1. Introduction

The NiTi shape memory alloy (SMA) with an approximately equal atomic ratio is a kind of novel functional materials which has the ability to return to a previously defined shape and size when subjected to the appropriate thermal procedure. These materials can be plastically deformed at a relatively low temperature , and will return to their shapes prior to the deformation during exposure to a higher temperature. Actually the NiTi SMA is unique memory alloy materials with extensive applications (Hwang, C.M., et al., 1983; Ling, H.C. et al., 1980, 1981; Nishida, M., et al., 1986; Miyazaki, S., et al., 1988).

Until now, people have not known what the behavior of NiTi alloy will be when decreasing the grain size to nanometer. No reports have been published on the local structure of nonoscale NiTi alloy. On the other hand, determination of the atomic structure of nanoscale solids is very important for understanding the properties of nano-materials. In the past decades, a huge number of investigations on the characteristic and the microstructure of nano-materials have been presented using various methods of structural analysis. Among them, extended x-ray absorption fine structure (EXAFS) is a powerful tool for identifying the local structure around the absorbing atoms. In this paper, the NiTi SMA was chosen as a target material to prepare the NiTi nanocrystal, then the local structure around Ni atoms was studied using the combination of EXAFS and XRD.

2. Experiments

The raw nano-NiTi powder, with a particle size of 7 nm, was synthesized using DC sputtering on a dedicated apparatus, which was named as "glow discharge-condensation-in situ pressure", and set up by Institute of Solid State Physics, Chinese Academy of Sciences (Zhu, Y., 1994), then condensed, and finally shaped with a pressure of 1.5 GPa. The target materials is a bulk NiTi SMA with bcc structure. A series of samples with different particle size were prepared by annealing the raw powder in vacuum at 400, 600 and 800°C respectively. EXAFS measurements at the Ni K-edge were performed in the transmission mode at the EXAFS station on beamline 4W1B of the Beijing Synchrotron Radiation Facility (BSRF). The storage ring operated at 2.2 GeV and 40-50 mA. Data analysis was performed using the EXCURV92 program. X-ray diffraction measurements were performed at beamline 4B9A of BSRF. A x-ray diffractomator with the precision of 0.001 degree is the main equipment. The incident beam intensity was monitored with an ion chamber and the diffracted intensity was detected by NaI(Tl) scintillation detector. There were two slits of 0.5 mm on the light path, one was set at the entrance of the beam and the other was at the front of the detector. The incident focused and monochromatic x-ray beam was calibrated by the Cu K-edge (1.54 Å). The energy resolution $\Delta E/E$ was 4×10^{-4}.

3 Results and discussion

3.1 XRD

From transmission electron microscopy (TEM) experiments, it was found that the NiTi grains grow in size when the annealing temperature increases, and finally their particle size increases to about 20 nm by raising the temperature to 800°C (X. Ju et al. 1995).

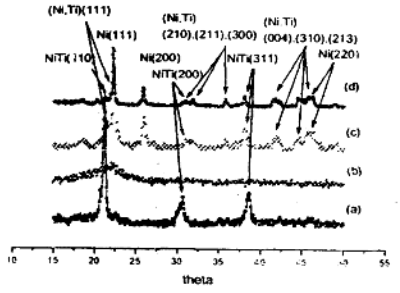

Fig. 1 X-ray diffraction patterns of nano-NiTi samples. (a) NiTi alloy; (b) as-grown NiTi powder; (c) annealing at 400°C; (d) annealing at 600°C

The as-grown NiTi powder was prepared by the DC sputtering method using NiTi SMA target with the bcc structure. Figure 1 shows the XRD pattern of the target material. Three strong peaks are attributed to (110), (200) and (211) as indicated in Fig 1(a). Fig. 1(b) shows the diffraction pattern of the as-grown NiTi powder. There is a broad peak corresponding to non-crystalline materials. Figures 1(c) and (d) correspond to the samples obtained by annealing at 400 an 600°C respectively. The structure of these samples identified from the diffraction patterns is not the same as the bcc structure of the target material. At first, it can be exhibited a group of strong diffraction peaks of Ni with a cubic structure. As indicated in Fig. 1(c) and (d), the strongest peak is at θ=22.2 for (111), the peaks at θ=25.6, 38.0 and 46.4 are identified as the (200), (220) and (311) of Ni crystalline with a cubic structure. Meanwhile, it should be pointed out that two groups of weak peaks exist and are corresponding to target material and the (Ni,Ti) type alloy with hexagonal structure, which is atomic occupation in random. As indicated, the peak at θ=30.1

for (200) of NiTi alloy with a bcc structure can be observed, but the peaks at θ=21.1 for (110) and 38.6 for (211) emerge with those of Ni crystalline with a cubic structure.For the (Ni,Ti) type alloy with hexagonal structure, there is a similar behavior that the strongest peaks at θ=22.0 for (111) is overlapped with the (111) of Ni crystalline. Three weak peaks at θ=41.5, 44.6 and 45.7 can be assigned to (004), (310) and (213) of this alloy. Moreover, there are three small peaks at θ=31.1, 32.9 and 35.8, and can be identified to (210), (211) and (300) of the hexagonal structure of (Ni,Ti) alloy. On the other hand, the diffraction intensity of the bcc phase is much weaker than the one of the crystalline as indicated.

Finally the above phenomena mean that a large fraction of Ni atoms were separated out in the sputtering process. On the other hand, the diffraction intensities of the bcc- and hexagonal phase of NiTi alloy were much weaker than that of the Ni crystalline as shown in Fig. 1.

3.2 EXAFS

The Fourier Transforms of the EXAFS spectra, and the structural parameters determined by fitting with EXCURV88 for various NiTi nanocrystalline samples are shown in Fig. 2 and Table 1. It was found that there are four Ti atoms and two Ni atoms around central Ni atoms, and the bond length of Ni-Ti and Ni-Ni were 0.2462 nm and 0.2585 nm after annealing at 800°C It is consistent with the conclusion attracted from the XRD experiments, in which a large fraction of Ni crystalline was separated out after the sputtering process. Meanwhile the structure was relaxed because the atomic occupation is random in the (Ni,Ti) alloy with a bcc- and hexagonal structure,. The experimental values of Ni-Ti and Ni-Ni interatomic distances were deviated from those of Ni-Ti alloy and the Ni crystalline presented in the PDF cards. From the amplitude of the overlapping Ni-Ni and Ni-Ti peak, it is found that the coordination number (CN) increases with rising the annealing temperature and the Ni-Ti and Ni-Ni distances come to keep stable. On the other hand, the higher shell peaks disappear rapidly and the degree of disorder increases with decreasing the annealing temperature, which can be interpreted that the long range order in the structure has been destroyed with the decreasing of the particle size.

Table 1 The structural parameters fitting with EXCURV88 Program

Condition	Distance (nm)		Coordination Number		Debye-Waller factor (10^{-3})	
	Ni-Ti	Ni-Ni	Ni-Ti	Ni-Ni	Ni-Ti	Ni-Ni
Raw powder	0.2398	0.2586	2.3	0.8	3.7	4.8
Annealed at 400°C	0.2463	0.2583	4.0	1.3	3.9	4.0
Annealed at 600°C	0.2459	0.2580	3.8	1.8	2.0	2.0
Annealed at 800°C	0.2462	0.2585	4.2	1.8	1.7	1.7

These structural changes can be attributed to the preparation of the nano-NiTi with the sputtering method. As known, there is a very high internal energy of the system in plasma heating, and most of chemical bonds of NiTi SMA as target materials are broken. Finally the Ti and Ni atoms are evaporated and deposited randomly on the substrate. A weak bonding between Ni and Ti atoms can be formed when the temperature of the plasma is lower since a strong bonding in plasma is impossible,. Therefore the bcc- and hexagonal phase are observed in the nano-(Ni,Ti) alloy when annealing at different temperatures. Moreover, it is known that eight Ti atoms are around each Ni atom in the NiTi SMA with bcc structure. According to the results of EXAFS and XRD experiments, the phase transition occurs from bcc- to hexagonal-structure in the synthesis process of the as-grown NiTi powder, and the structural relaxation also does. So their structural parameters should be changed. To sum up, the Ni and Ti atoms on a little ultrafine alloy particles produced by sputtering at the beginning are cooled and deposited in disorder on the substrate. Among them, ultrafine alloy particles are of the initial bcc structure. Following, with the increase of annealing temperature, the (Ni,Ti) type alloy with the atomic occupation in random is produced with the hexagonal structure except the formation of crystalline.

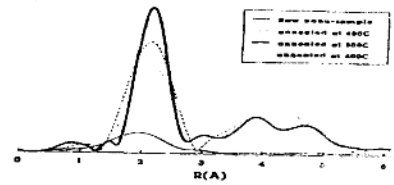

Fig. 2 RDF of Ni-K-edge

It is reported that the Ni_3Ti phase with nano-dimension will result in the serious decay of SMA performance and further fracture of the SMA material (Wen, S.L. et al., 1999). In our experiment, no Ni_3Ti phase was observed.

4. Conclusion

The structures of NiTi nanocrystals with different annealing temperatures, prepared by sputtering method,. were different from bulk NiTi alloy with bcc structure as target materials. When increasing the annealing temperature, a small fraction of the (Ni,Ti) type nanocrystal with the hexagonal structure was presented except target materials and Ni crystalline, and it is atomic occupation in random.

Reference

Hwang, C.M., Meichle, M., Salamon, M.B. and Wayman, C.M., (1983) Phil. Mag. 47A, 31

Ju, X., Su, Y. X., Su, T. D., Zhu, Y. and Shi, C. S., (1995) J. USTC, 25, 169

Ling, H.C. and Kaplow, R., (1980). Metall. Trans. 11A, 77; (1981) Mat. Sci. Engr. 48,241

Miyazaki, S., Kimura, S. and Otsuka, K., (1988) Phil. Mag. A57, 467

Nishida, M., Wayman, C.M. and Honman, T., (1986) Metallography, 19, 99

Wen, S. L and He, J. B., (1999) J. Func. Mat. Device. 5, 303

Zhu, Y., (1994) Physics, 23, 111

Received 31 July 2000 · Accepted 4 December 2000

Preparation and photoluminescence of nanowire array and films of cadmium sulfide by electrodepositing in organic solvent

X. Ju[1], L. Q. Peng

BSRF, Institute of High Energy Physics, CAS, Beijing 100039, P. R. China

ABSTRACT

Nanowire array and film of cadmium sulfide were prepared by electroplating in organic solvent dimethyl sulfoxide with $CdCl_2$ and element sulfur under different temperature and current density. The UV-VIS absorption spectra show that increasing the electroplating temperature is benefit to forming perfect crystallites and the absorption peak under high electroplating temperature is ascribed to the excitonic transition. The formula of energy shift for the lowest several excitons is given and compared with the experiment. The photoluminescence spectrum consists of two parts: the first is produced by recombination of the defects and the second by recombination of excitons.

Keywords: CdS, nanowire array, electroplating

1. INTRODUCTION

The nature of semiconductor nanomaterials is situated between that of the corresponding molecules and bulks. The change of their physical and chemical properties is noticeable to follow their dimension[1]. Semiconductor cadmium sulfide (CdS) is of the remarkable effect of quantum size. There are lots of experiments to investigate the relationship between the optical absorption, photoluminescence and the micro-crystallites size. It indicates that the features of the photoluminescence spectroscopy for CdS nano-crystallite, which grows in zeolite, polymer and glass, depends on the preparation of samples[2] and reflects the information on the impurity, defect and surface state[3]. Since A. S. Baranski etc. obtained the II-VI group semiconductor in organic solvents with the electrodepositing method[4], a series of investigations on their preparation, behavior and applications such as solar cell have been carried out [5]. Generally, the CdS nano-crystalline preparing in chemical reaction at room temperature, sometimes with the annealing, is embraced by inert surface or embedded in the isolated materials. But, it is different that the CdS nano-crystalline is electroplated in organic solvent at higher temperature, which is of the metal-like multi-crystallite structure without the impurities.

On the other hand, template synthesis is an elegant chemical approach for the fabrication of nanowires and has attracted more and more attention. Arrays of metal[6-8], semiconductor[4], conducting polymer[9] nanowires and carbon nanotubes[10] are obtained by electrodepositing or other methods in porous templates such as anodic aluminum oxide films and nuclear track membranes. Applications of these materials include arrays of electron field emitters[11], nanoelectrodes for electrochemical experiments[12], magnetic sensors based in the giant magnetio-resistance effect[13] and anisotropic optical filters[14].

Although CdS nanowire arrays with diameter as small as 9nm have been fabricated in anodic aluminum oxide films with the oxide barrier layer separating the Al substrate and the porous aluminum oxide[5], there is a main constraint in the experiments such as absorption spectra in order to separate CdS nanowire arrays from the Al substrate. However, the characterization of CdS nanowire arrays can be studied thoroughly if they are fabricated in nuclear track membranes. In this paper, we report the fabrication and optical characterization of CdS nanowires with a diameter of 200nm in nuclear track membranes and the corresponding films under the same or different conditions by electroplating in organic solvent dimethylsulfoxide (DMSO).

2. EXPERIMEMTAL

[1] Correspondence: jux@ihep.ac.cn; Telephone: 86-10-68235998; Fax: 86-10-68186229

Micromachining and Microfabrication Process Technology and Devices, Norman C. Tien, Qing-An Huang, Editors, Proceedings of SPIE Vol. 4601 (2001) © 2001 SPIE 0277-786X/01/$15.00

Commercial polyethylene-terephthalate (PET) film from Japan with a thickness of 16μm was irradiated at the tandem accelerator of China Institute of Atomic Energy, Beijing, with sulfur ions (4.1MeV/amu) with a fluence of 3×10^8 ions per cm^2. The ion irradiated PET film was UV irradiated for track sensitization. The film was then sensitized with ammonia water moreover. Etching was performed with a 0.5N NaOH aqueous solution at 73°C to produce membranes with a pore diameter of 0.2μm. A 20nm gold layer was sputtered onto one side of the membrane serving as the working electrode. A 3μm nickel film was then electroplated on the gold surface of the membrane so that the electrode completely covered and sealed the pores of the membrane. Deposition of CdS into the pores of the membrane was carried out galvanostatically (current density = 2.0 mA/cm^2, time = 40 min) in a solution that contained 0.055M $CdCl_2$ and 0.19M elemental sulfur dissolved in DMSO at 110°C. The solution was stirred with a magnetic stirrer during deposition. A film of CdS was also deposited on Al substrate under the same condition in order to produce the sample 1 for comparison. On the other hand, the samples 2, 3 were prepared at 125°C under different the current density, 3.0mA/cm^2 and 5.0mA/cm^2, respectively.

The scanning electron microscope (SEM) experiments for both nanowire array and films were carried out on Hitachi S-450 instrument operated at 20 kV and equipped with energy dispersive X-ray (EDX) fluorescence microanalysis in order to obtain morphological information and the atomic composition of the semiconductor samples. The sample of CdS nanowire array for the SEM was prepared by dissolving the membrane in a solution composed of KOH, water and ethanol at room temperature for a long time. The crystal structure of the samples was analyzed by a D/max-RB diffractometer with Cu K_α radiation.

The sample of CdS nanowire array for optical experiments was prepared by removing the metal layer from the membrane by polishing. The samples of CdS films as contrast were removed from the Al substrate by attaching the exposed face of the CdS films to a transparent adhesive tape and then dissolving the Al substrate in a NaOH aqueous solution (6.8N). Absorption spectra were taken using a Beckman BU-600 spectrophotometer at room temperature. Photoluminoscence spectra were measured with a PERKIN ELMER LS50B luminescence spectrometer.

3. RESULTS AND DISCUSSION

3.1. SEM and XRD

The images of CdS nanowire array and films are shown in Fig.1. For the samples of CdS nanowire array, it is apparent that the deposited semiconductor fills the pores uniformly and continuously, which means the semiconductor faithfully reproduce the shape of the pores. It is also revealed that the nuclear track membrane suppresses the morphology with significant cracking, typical of electrodeposited CdS in DMSO[4]. Thus template restriction of the growth dimensions can improve the overall morphology of electrodeposited semiconductor materials. In addition, the sample 1 consists of granular structure with crackles; the samples 2 and 3 are close to the crystallites with holes. These indicate that the samples crystallize well at higher temperature. The semiquantitative analysis of CdS nanowire array by EDX gives a composition of 50.1 at % Cd, 45.7 at% S and 4.2 at% Cl. For a comparison, the atomic composition of the films is similar to that of the nanowire array. But, the Cd content of the sample 3 is stoichiometric excess, about 2%, meanwhile, there is a trace of elemental Cl, <4%.

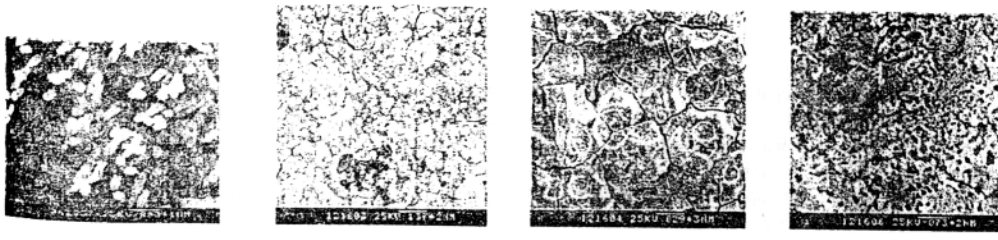

(a) (b) (c) (d)

Fig 1. The SEM images of CdS nanowire array and films. (a) the nanowire array sample, 110°C, 2.0mA; (b) the film sample 1, 110°C, 2.0mA; (c) the film sample 2, 125°C, 3.0mA; (d) the film sample 3, 125°C, 5.0mA

The x-ray diffraction peaks of the sample of CdS nanowire array and films could be assigned to the hexagonal greenockite phase CdS, Ni, Au and nuclear track membrane, without any trace of elemental Cd or S. Additionally, in the calculation of the crystallite size, the effect of the non-uniform stress in CdS should be removed[15]. Analysis of the width of the peaks using the Debye-Scherrer formula indicates that the crystallite size of CdS in the nanowire array sample is on the order of 10-20nm when neglecting the stress effect, similar to those in CdS films[16]. Here, as reference, the average crystallite size of the sample 1 was estimated to be about 20 nm. Similarly, that of both the sample 2 and 3 is about 10nm.

3.2. UV-VIS spectra

The absorption spectrum of CdS naonowire array and films are shown in Fig.2. The optical band gap of all samples is 515.5nm (2.40eV), and corresponds well to that of CdS. All of this together with the available data on the electrodepositing of CdS from DMSO[4,15,16] makes us confident that the deposited material in nuclear track membrane is n-CdS doped with Cd and Cl. For CdS nanowire array, the most striking feature is that there is a well-developed maximum at the wavelength of 690 nm, located in lower energy side of the onset of absorption. The onset of absorption shows no shift to that of the CdS films[16]. On the other hand, the samples 2 and 3 are of distinguishing peak of exciton at higher side of the onset of absorption[2]. The positions of the absorption of both samples are at 485.5nm with a FWHM of 0.35eV and 489.7nm with a FWHM of 0.2eV, resepctovely. Moreover, there is a shoulder at 459nm for the sample 3. Compared to colloid CdS[2], the crystallite size of the samples 2 and 3 is about 10nm, and that of the sample 1 is little bigger and close to the estimated value by XRD.

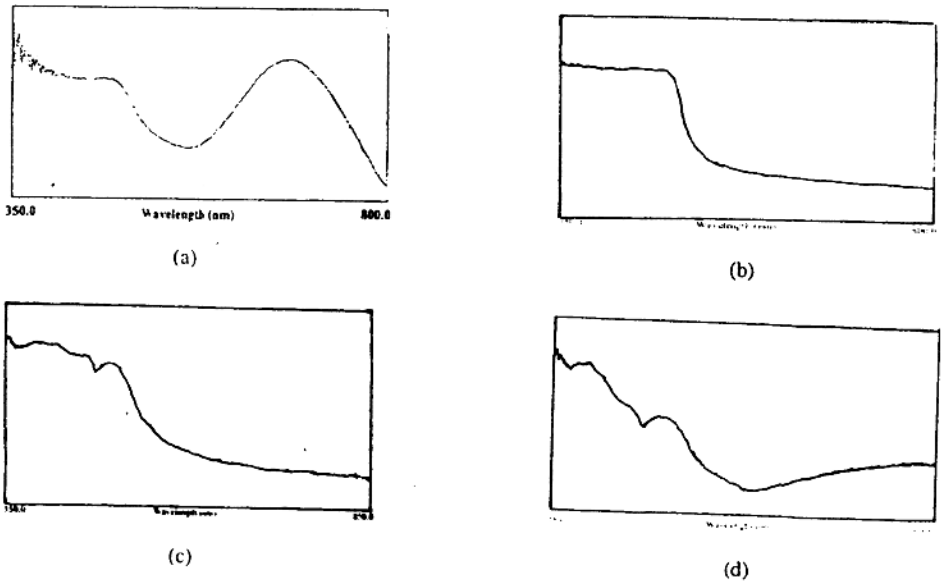

Fig.2. The absorption spectra of sample of CdS nanowire array and films. (a) the nanowire array sample; (b) the film sample 1; (c) the film sample 2; (d) the film sample 3

3.3. Photoluminescence spectra

The photoluminescence spectra of the CdS nanowire array and the film are shown in Fig.3, accompanying with the exciting spectrum of the sample 1 since that of all samples is almost identical. The spectrum of the CdS sample 1 shows three broad emission bands that have three major peaks at 530, 590 and 660nm, respectively. For the band at 530nm, it is 0.6eV below the onset of absorption and not occurred in CdS nano-crystallite prepared in chemical reaction. Considering the existence of Cl ion in the electrodeposited CdS films, which acts as a shallow donor and contributes to the very high electron density[15], it is ascribed to originate from the recombination of the energy level of the donor. The

spectrum of the CdS nanowire array shows similar structure except for indistinct peaks at 530mn and 590nm due to low signal to noise ratio. Both the 590 and 660nm broad bands can be observed in photoluminescence spectra of CdS clusters and attributed to Cd atoms and sulfur vacancy, respectively[3, 17]. From the analysis of atomic composition, Cd atoms and sulfur vacancy should also exist in the samples of CdS nanowire array and films. Thus we assign the 590mn and 660nm bands to Cd atoms and sulfur vacancy respectively. For sample 2 and 3, there are two narrow bands at 486 and 460nm with a FWHM of 0.04eV, which corresponds to that of the absorption spectra and is from the recombination of the bound-exciton.

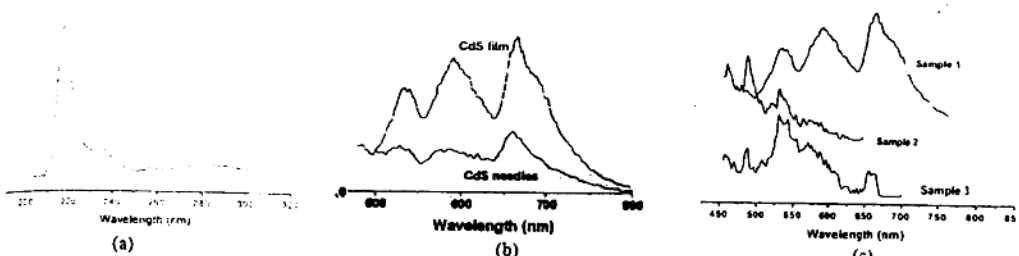

Fig.3. The photoluminescence spectra of the samples of CdS nanowire array and films. (a) the exciting spectrum of film sample 1; (b) the nanowire array sample and the film sample 1; (c) the film sample 1-3

Because of the size effect in nanocrystalline, the exciton is bound with higher energy and intensity, so the absorption of exciton can be presented at room temperature. Under the approximation of effective mass, the relationship between energy shift of the lowest energy exciton, ΔE, and radius, R, is as follows:

$$\Delta E = \frac{\hbar^2\pi^2}{2R^2}[\frac{1}{m_e}+\frac{1}{m_h}]-\frac{1.786e^2}{\varepsilon \cdot R}-0.248E^*_{Ry},$$

in which the first term is the kinetic energy of the minimum quantization in rectangular potential well; m_e and m_h is the mass of electron and hole, respectively. The second term is the Coulomb potential between electron and hole. ε is dielectric constant. The third term is the correlation energy, and very small in common. Generally, there is a big difference between the formula and experiments when R is small, but the calculation is consistent with experiments in the region of 3-4nm[18,19]. Supposed that m_e=0.165m and m_h=0.98m (m: the mass of electron) and ε=5.5[3], the calculated radius with this formula is 4nm at the lowest exciton energy, 498nm, and very close to results from XRD experiments. Regarding the common expression of the quantization energy of particle in rectangular potential well[20], ΔE can be shown:

$$\Delta E = \frac{\hbar^2k^2_{l,m}}{2R^2}[\frac{1}{m_e}+\frac{1}{m_h}]-\frac{1.786e^2}{\varepsilon \cdot R}-0.248E^*_{Ry},$$

in which the $k_{l,m}$ is quantum number, as known, $k_{1,0}$=3.14, $k_{1,1}$=4.49, $k_{1,2}$=5.76. The calculated second lowest energy of exciton is 457nm with a radius of 4nm, and in accordance with our experimental value, 460nm.

There is no absorption of exciton for the sample 1. This is because its size is bigger and the intensity is weaker[2,21]. On the other hand, it may concern the imperfect growth of crystallites at lower temperature in electrodepositing process. In our experiment, the onset of absorption of the CdS films, prepared the materials at 100°C under different current density, shifts blue 2.60eV without absorption of exciton, which indicates the electrodepositing temperature is of a great impact on the optical properties of CdS nanomaterials. Additionally, when the amorphous CdS, electrodepositing at room temperature, is annealed at 600°C, the crystallization is still worse than that at 100°C, which means that the electrodepositing temperature is more important than the annealing one. Compared to results of reference 4, the photoluminescence of the samples 2 and 3 are stronger with the same crystallite size. It may attribute that different electrodepositing temperature results in different degree of crystallization. The photoluminescence of sample 2 is stronger than that of sample 3, which shows that the crystallization of semiconductor is better when electrodepositing with a weaker current

density at the same temperature[22]. Consequently, the change of photoluminescence is also related to the perfection of crystallite.

As described above, there are same native defects and impurity defects in the sample of CdS nanowire array and CdS film sample, which eliminates the possibility that the absorption peak in Fig.2 is ascribed to the defects. Additionally, there is no sharp emission band with peak at 690nm in the photoluminescence spectrum of the sample of CdS nanowire array, which eliminates the bound-exciton as the possible mechanism for the absorption peak. Considering that there are a number of interface states between the CdS nanowire array and the membrane pores, we therefore assign it to the interface states transition. This is also supported by the following facts: the typical value of semiconductor surface potential 0.5V[23] is near the 0.6eV difference value between the absorption peak and the onset of absorption; the recombination by surface states is a radiationless relaxation process.

4. CONCLUSION

It can be concluded that (1) CdS nanowire array with a diameter of 200nm have been fabricated by electrochemical deposition in nuclear track membrane. An intense absorption peak of the CdS nanowire array was observed and it could be assigned to transition of the interface states; (2) increasing the electrodepositing temperature is favor to grow nanocrystallites with perfect structure, and results in the absorption of exciton; (3) the formula for the secondary lowest energy shift is given, and consistent with our experiments; (4) the spectra of photoluminescence is composed of bands from the recombination of impurity, defect etc., in which the bands from the stronger recombination of exciton corresponds to that of the bound-exciton. Finally, their intensity is related to the perfection of crystallite.

REFERENCES

1. A. P. Alivisatos, "Semiconductor Clusters, Nanocrystals, and Quantum Dots," *Science*, **27**, pp. 1933-937, 1996
2. T. Vossmeyer, L Katsikas, M. Giersig, I. G. Popovic, K. Diesner, A. Chemseddine, A. Eychmuller, H. Weller, "CdS nanoclusters: Synthisis, characterization, size-dependent oscillator strength, temperature shift of the excitonic transition energy, and reversible absorbance shift," *J. Phys. Chem.* **98**, pp. 7665-7673, 1994
3. Y. Wang and N. Herron, "Photoluminescence and relaxation dynamics of CdS superclusters in zeolites," *J. Phys. Chem.* **92**; pp. 4988-4994, 1988
4. A.S Baranski, W.R Fawcett, A. C. McDonald and R.M. de Nobriga, "The structural characterization of Cadmium Sulfide films gown by cathodic electrodeposition," *J. Electrochem. Soc.* **128**, pp. 963-968, 1981
5. D. Routkvitch, T. Bigioni, M. Moskovits and J. M. Xu, "Electrochemical fabrication of CdS nanowire arrays in porous anodic aluminum oxide," *J. Phys. Chem.* **100**, pp. 14037-14047, 1996
6. C. R. Martin, "Nanomaterials: a membrane-based synthetic approach," *Science*, **266**, pp. 1961-1966, 1994
7. L. Wang, K. Yu-Zhang, A. Metrot, P. Bonhommc and M. Troyon, "TEM study of electrodeposited Ni/Cu multilaycrs in the form of nanowires," *Thin solid Film*, **288**, pp. 86-89, 1996
8. C. Schonenberger, B. M. I. van der Zande, L. G. J. Fokkink, M. Henney, C. Schmidt, M. Krugel, A. Bachtold, R. Huber, H. Birk and U. Staufer, "Template synthetic of nanowires in porous polycarbonate membranes: electrochemistry and morphology," *J. Phys. Chem.* **B101**, pp. 5497-5505, 1997
9. L. Piraux, S. Dubois and S. Demoustier-Champagne, "Template synthetic of nanoscale materials using the membrane porosity," *Nucl. Instrum. Meth.* **B131**, pp. 357-363, 1997
10. W. Z. Li, S. S. Xie, L. X. Qian, B. H. Chang, B. S. Zhou, W. Y. Zhou, R. A. Zhao and G. Wang, "Large-scale synthesis of aligned carbon nanotubes," *Science* **274**, pp. 1701-1703, 1996
11. W. A. de Heer, A. Chatelain and D. Ugarte, "A carbon nanotube field-emission electron source," *Science*, **270**, pp. 1179-1180, 1995
12. V. P. Menon and C. R. Martin, "Fabrication Md evaluation of nanodectrodes ensembles," *Anal. Chem.* **67**, pp. 1920-1928, 1995
13. L. Piraux, J. M. George, J. F. Despre, C. Leroy, E. Ferain, R. Legras, K. Punadjela and A. Fert, "Giant magnetoresistance in magnetic multilayered nanowires," *Appl. Phys. Lett.* **65**, pp. 2484-2486, 1994
14. C. A. Foss, G. L. Hornyak, J. A. Stockert and C. R. Martin "Template synthetic of nanoscopic gold particles: optical spectra and the effects of particle size and shape," *J. Phys. Chem.* **98**, pp. 2963-2971, 1994
15. A. S. Baranski, M. S. Bennett and W. R. Fawcett, "The physical properties of CdS thin films electrodeposited from aqueous diethylene glycol solution," *J. Appl. Phys.* **54**, pp. pp. 6390-6394, 1983

16. E. Fatas, P. Herrasti, F. Arjona, E. G. Camarero and J. A. Medina, "Electrodepositing and characterization of CdS thin films on stainless steel and tin oxide substrates," *Electrochimica. Acta*, **32**, pp. 139-148, 1987
17. J. J. Ramsden, S. E. Webber and M. Gratzel, "Luminescence of colloidal CdS particles in acetonitrile and acetonitrile/water mixtures," *J. Phys. Chem.* **89**, pp. 2740-2743, 1985
18. P. E. Lippens and M. Lannoo, "Calculation of the band gap for small CdS and ZnS crystallites," *Phys. Rev.* **B39**, pp. 10935-10942, 1989
19. Y. Wang and N. Herron, "Quantum size effects on the exciton energy of CdS clusters," *Phys. Rev.* **B42**, pp. 7253-7255, 1990
20. J. X. Fang and D. Lu, *Solid State Physics*, Scientific and Technological Press, Shanghai, 1981
21. Y. Kayanuma, "Quantum-size effects of interacting electrons and holes in semiconductor microcrystals with spherical shape," *Phys. Rev.* **B38**, pp. 9797-9805, 1988
22. A. C. Rastogi and K. S. Balakrishnan, "Monocrystalline CdTe Thin Films by Electrochemical Deposition From Aprotic Electrolytes," *J. Electrochem. Soc.* **136**, pp. 1502-1505, 1989
23. K. Seeger, *Semiconductor Physics*, Springer-Verlag, Wien, 1973

SURFACE AND INTERFACE ANALYSIS
Surf. Interface Anal. 2001; **32**: 95–97

SIA

Evidence for change of the interfacially local structure of titanium oxide/bis[(4,4′-carboxy-2,2′-bipyridine)(thiocyanato)] ruthenium nanocomposite†

X. Ju,[1]* J. Zhang,[1] K. W. Wu,[2] Y. J. Hou,[2] P. H. Xie[2] and B. W. Zhang[2]

[1]Institute of High Energy Physics, Chinese Academy of Sciences, Beijing 100039, P.R. China
[2]Institute of Photography, Chinese Academy of Sciences, Beijing 100101, P.R. China

Received 23 October 2000; Revised 7 December 2000; Accepted 9 January 2001

Titanium oxide/bis[(4,4′-carboxy-2,2′-bipyridine)(thiocyanato)]ruthenium (*cis*-$(NCS)_2RuL_2$) nanocomposites were prepared by the self-assembly method. In this system, their interfacially local structures were probed by x-ray absorption spectroscopy (XAS) and the Ti–O interatomic distance and the coordination number of the O atoms around the Ti central atoms were extracted. Compared with TiO_2 nanoparticles, the Ti local structure in the nanocomposite was changed, which is responsible for binding *cis*-$(NCS)_2RuL_2$ to the surface of TiO_2 nanoparticles. Copyright © 2001 John Wiley & Sons, Ltd.

KEYWORDS: XAS; TiO_2/*cis*-$(NCS)_2RuL_2$ nanocomposite

INTRODUCTION

A new type of photovoltaic cell was reported recently based on spectral sensitization of thin nanocrystalline TiO_2 (anatase) films by ruthenium polypyridine complex chromophores.[1] Generally, interfacial electron transfer from photoexcited states of the chromophore into the conduction bands of the semiconductor depends on a number of factors. The structural and electronic properties of the interface are very important[2] but they are not completely clear. The techniques of x-ray absorption near-edge structure (XANES) and extended x-ray absorption fine structure (EXAFS)—together called x-ray absorption spectroscopy (XAS)[3]—are atom specific and capable of probing the short-to-medium range structure around an imbedded or absorbing atom,[4] which can provide the structural origin of the unique photoelectronic property of the nanocomposite. In this work, we prepare a TiO_2/bis[(4,4′-carboxy-2,2′-bipyridine)(thiocyanato)]ruthenium (*cis*-$(NCS)_2RuL_2$) nanocomposite by the self-assembled method, and present our recent XAS study on the Ti K-edge on TiO_2 nanoparticles of 10–20 nm without and with an assembly of *cis*-$(NCS)_2RuL_2$. Surface distortion of the Ti in the TiO_2 nanoparticles and the interfacial interaction between TiO_2 and *cis*-$(NCS)_2RuL_2$ are discussed.

EXPERIMENTAL

The TiO_2 film was prepared by casting 11% TiO_2 nanoparticles of size 10–20 nm on the glass substrate and heat treating at 450 °C for 30 min. The TiO_2/*cis*-$(NCS)_2RuL_2$ nanocomposite was obtained by dipping the TiO_2 film into the *cis*-$(NCS)_2RuL_2$ ethanol solution for 24 h[5] and then drying for 2 days. The XAS spectra at the Ti K-edge were measured in transmission mode by using synchrotron radiation with a Si(111) double-crystal monochromator on the EXAFS station at the 4WIB beamline of Beijing Synchrotron Radiation Facility (BSRF). The storage ring was operated at 2.2 GeV with a beam current of ~80 mA. The energy resolution was 1.5 eV for the near-edge structure and ~3.0 eV for the EXAFS. Data analysis were performed in the EXCURV88 program.

RESULTS

X-ray absorption near-edge structure

The XANES spectra at the Ti K-edge of bulk TiO_2, TiO_2 nanoparticles and TiO_2/*cis*-$(NCS)_2RuL_2$ nanocomposites are shown in Fig. 1. As is known, the XANES spectrum contains several well-defined pre-edge peaks that are related to the local structure surrounding Ti atoms. For bulk TiO_2 (anatase), it exhibits three small pre-edge peaks (A_1, A_2, A_3) that are assigned respectively to transitions from the 1s core level of Ti to $1t_{1g}$, $2t_{2g}$ and $3e_g$ molecular orbitals.[4] On the other hand, the intensities of these pre-edge features are a strong function of the distortion of the oxygen octahedron around the central absorbing Ti atom. For TiO_2 nanoparticles, an increase in the intensity of the A_2 peak is observed, indicating an increasing distortion from the oxygen octahedron that may result from the surface effect of TiO_2 nanoparticles.[4] However, there is very little effect of the *cis*-$(NCS)_2RuL_2$ assembly on the XANES spectrum for TiO_2 nanoparticles.

*Correspondence to: X. Ju, Institute of High Energy Physics, Chinese Academy of Sciences, Beijing 100039, P.R. China.
E-mail: jux@alpha02.ihep.ac.cn
†Paper presented at APSIAC 2000: Asia–Pacific Surface and Interface Analysis Conference, 23–26 October 2000, Beijing, China.

DOI: 10.1002/sia.1014

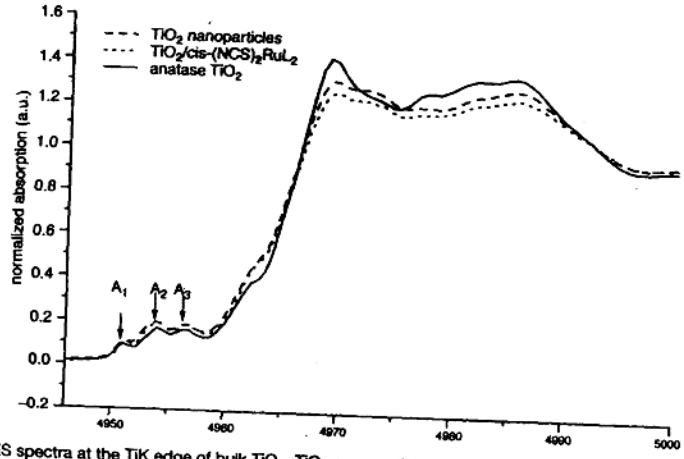

Figure 1. The XANES spectra at the TiK edge of bulk TiO_2, TiO_2 nanoparticles and TiO_2/*cis*-$(NCS)_2RuL_2$ nanocomposites.

Extended x-ray absorption fine structure

The radial distribution functions (RDF) of TiO_2 nanoparticles and the TiO_2/*cis*-$(NCS)_2RuL_2$ nanocomposite are shown in Fig. 2. The fitting results are listed in Table 1, along with the standard crystalline TiO_2 in anatase phase.

For all samples, the first-shell Ti–O peak in the Fourier transform EXAPS spectra was fitted on a two-subshell model. The bond lengths r_1 and r_2 of two Ti–O subshells of TiO_2 nanoparticles and TiO_2/*cis*-$(NCS)_2RuL_2$ nanocomposite are different from that of the reference standard. It is well known that the structure of nanomaterials is relaxed from the perfect crystal structure to the local structure with amorphous features. For most nanomaterials, the interatomic distance become shorter as the particle size decreases, but the bond

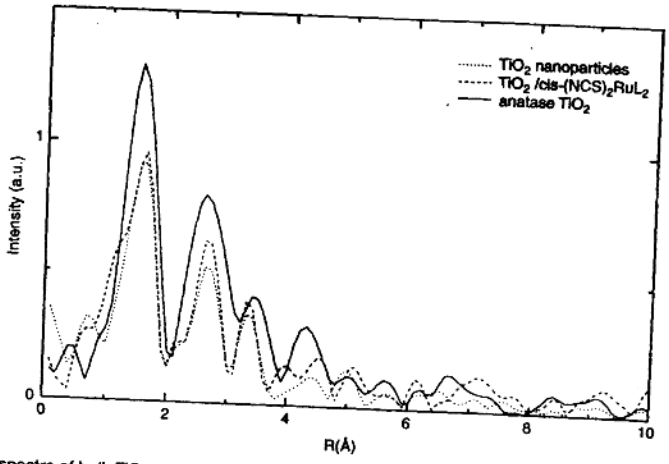

Figure 2. The EXAFS spectra of bulk TiO_2, TiO_2 nanoparticles and TiO_2/*cis*-$(NCS)_2RuL_2$ nanocomposites.

Table 1. Fitting of the EXAFS parameters with EXCURV88

Sample	E_0	r_1(nm)	r_2(nm)	n_1	n_2	a_1	a_2
TiO_2 (anatase)[a]	8.479	1.906	1.936	4.0	2.0	—	—
TiO_2 nanoparticles	12.87	1.880	1.909	4.0	1.6	0.02026	0.01189
TiO_2/*cis*-$(NCS)_2RuL_2$	11.94	1.857	1.901	2.7	2.2	0.01097	0.00972

[a] The structural data were extracted from the PDF cards.

length of the first subshell of the TiO_2/*cis*-$(NCS)_2RuL_2$ nanocomposite has an observable change compared with that of TiO_2 nanoparticles.

From the point of view of atomic coordination, the coordination numbers n_1 and n_2 of the O atoms around the Ti central atoms in the TiO_2 nanoparticles are 4.0 and 1.6, which is a little less than those of the reference standard (n_1 = 4.0, n_2 = 2.0). Actually, this is consistent with the properties of the local structure of nanomaterials, because the particle size of nanoparticles is small and results in an incomplete atomic coordination of the surface atoms.[4] For the TiO_2/*cis*-$(NCS)_2RuL_2$ nanocomposite, the corresponding coordination numbers are 2.7 and 2.2. This reveals that the Ti local structure is reconstructed when *cis*-$(NCS)_2RuL_2$ is organized on the surface of the TiO_2 nanoparticles.

DISCUSSION

It should be pointed out that the above phenomena result from the assembly *cis*-$(NCS)_2RuL_2$ on the surface of the TiO_2 nanoparticles, which can be attributed to the COOH groups in dye molecules coordinating to the Ti atoms of TiO_2 nanoparticles. In general, it is easier to form a complex of Ti and COOH on a surface,[6] which would result in reconstruction of the Ti local structure. Therefore, compared with TiO_2 nanoparticles, the coordination number of the first subshell decreases and the bond length reduces[7] in the nanocomposite. Finally, the Debye–Waller factors a_1 and a_2 in Table 1 can describe the degree of disorder of the materials. It is found that the TiO_2/*cis*-$(NCS)_2RuL_2$ nanocomposite tends to have smaller values of such factors. As mentioned above, the COOH groups in the dye molecules are coordinated with the Ti atoms of the TiO_2 nanoparticles, and the complex relationship made the second subshell of the Ti–O full, which results in a modification and a smoothing of the surface of the TiO_2 nanoparticles.

CONCLUSION

In the composites studied here, *cis*-$(NCS)_2RuL_2$ is assembled onto TiO_2 nanoparticles. The COOH groups in dye molecules can be coordinated with the Ti atoms on the surface of TiO_2 nanoparticles, which is expected to modify significantly the local structure of the TiO_2 nanoparticles. This study provides structural evidence for the interfacial property of the nanocomposites and acts as a guide for the rational design of electronic–optical materials.

REFERENCES

1. Braginsky L, Shklover VJ. *Solid. State Commun.* 1998; 105: 701.
2. Shklover V, Ovchinnikov YE, Braginsky LS, Zakeeruddin SM, Gratzel M. *Chem. Mater.* 1998; 10: 2533.
3. Iwasawa Y. *X-ray Absorption Fine Structure for Catalysts and Surfaces*. World Scientific: New Jersey, 1996.
4. Luca V, Djajanti S, Howe RF. *J. Phys. Chem. B* 1998; 102: 10650.
5. Nazeeruddin MK, Kay A, Rodicio J, Humphrey-Baker R, Muller E, Liska P, Vlachopoulos N, Gratzel M. *J. Am. Chem. Soc.* 1993; 11: 6382.
6. Zhang J, Ju X, Wang BJ, Li QS, Hu TD, Liu T. *Synth. Met.* 2001; 118: 181.
7. Chen LX, Rajh TJ, Jager W, Nedelijkovic J, Thurnauer MC. *J. Synchr. Radiat.* 1999; 6: 445.